Black thin film silicon

Svetoslav Koynov,[a] Martin S. Brandt, and Martin Stutzmann
Walter Schottky Institut, Technische Universität München, 85748 Garching, Germany

(Received 11 May 2011; accepted 2 July 2011; published online 31 August 2011)

"Black etching" has been proposed previously as a method for the nanoscale texturing of silicon surfaces, which results in an almost complete suppression of reflectivity in the spectral range of absorption relevant for photovoltaics. The method modifies the topmost 150 to 300 nm of the material and thus also is applicable for thin films of silicon. The present work is focused on the optical effects induced by the black-etching treatment on hydrogenated amorphous and microcrystalline silicon thin films, in particular with respect to their application in solar cells. In addition to a strong reduction of the reflectivity, efficient light trapping within the modified thin films is found. The enhancement of the optical absorption due to the light trapping is investigated via photometric measurements and photothermal deflection spectroscopy. The correlation of the texture morphology (characterized via atomic force microscopy) with the optical effects is discussed in terms of an effective medium with gradually varying optical density and in the framework of the theory of statistical light trapping. Photoconductivity spectra directly show that the light trapping causes a significant prolongation of the light path within the black silicon films by up to 15 μm for $\sim$1 μm thick films, leading to a significant increase of the absorption in the red.
 [doi:10.1063/1.3626900]

I. INTRODUCTION

The development of thin film silicon solar cells is hindered by problems associated with the light-induced degradation of hydrogenated amorphous silicon (a-Si:H) and with the unsatisfactory efficiency of the usual p-i-n design of the cells. Two approaches for solving these problems are pursued at present: First, thinner p-i-n a-Si:H structures are used (with a thickness of less than 0.3 μm instead of the typical 0.5 to 1.0 μm),[1–3] which results in higher built-in electric fields and, consequently, a reduced degradation due to faster separation of the photogenerated carriers. Second, a-Si:H as the light absorbing material is substituted by the more stable microcrystalline silicon (μc-Si:H) (Refs. 4–8) or polycrystalline silicon.[9] The crystalline silicon phase has a weaker overall absorption, but this absorption matches the solar spectrum better.[4–6,9] A substantial challenge for both of these approaches is the low light absorption in the thin silicon films. Therefore, the development of efficient means of optical absorption enhancement becomes a task of crucial importance for further progress in this field.

It has been shown theoretically that a very strong absorption enhancement can be achieved by means of light trapping.[10,11] However, the high enhancement factors predicted theoretically are not reached by the solar cell structures used at present. In practice, all state-of-the-art thin-film silicon solar cells consist of corrugated p-i-n (or n-i-p) layer stacks, which are grown conformably over a textured substrate and are usually sandwiched between two layers of transparent conductive oxide (TCO). Thus all reflecting/scattering surfaces follow the topography of the substrate, usually defined by a texturing of the first TCO layer.[12] Considerable attention is currently given to the correlation of the light-trapping effects with the morphology of the TCO–Si interface.[12–16] In particular, it has been realized that the size of the features in the texture is important for the scattering mechanism at the interface and thus for the resulting light-trapping efficiency.[15] The typical features of the presently used textures have lateral sizes between several μm and $\sim$700 nm.[12–14] These sizes are larger than the effective wavelengths of the solar radiation in TCO that can be absorbed in silicon. Therefore, the optical phenomena at the TCO–Si interfaces employed so far are primarily governed by the rules of geometric ray optics. The resulting effects, beneficial for absorption enhancement in such structures, are mainly multiple reflection and scattering via refraction of the incoming rays at inclined surface facets, micro-focusing at lens-like surface profiles, etc.[13,14] These effects can be exploited effectively only by textures with a high aspect ratio (depth/lateral size), which would be impractically rough, with required texture depths in the micrometer range. It was also shown that silicon thin films grown over very rough surfaces become defective.[16] Another important limitation of this absorption enhancement approach is that the performance of the back reflectors, used to additionally improve the absorption, deteriorates with increasing roughness.[16] Therefore, the optimization of solar cells grown on textured substrates with respect to a geometrical absorption enhancement is a matter of compromise.

We previously developed a process for the nanoscale texturing of Si surfaces that results in an almost complete suppression of the reflectivity of these surfaces in the spectral range of Si absorption useful for photovoltaics.[17,18] The process, referred to as "black etching," is independent of the surface crystallographic orientation and affects only the topmost 150 to 300 nm of the Si material. We already have demonstrated that this process can be applied to bulk silicon

[a]Author to whom correspondence should be addressed. Fax: +49 89 289 12737. Electronic mail: koynov@wsi.tum.de.

of various structural modifications (single- or polycrystalline), as well as to thin a-Si:H films.[17] In the present work we discuss the optical effects induced in a-Si:H and μc-Si:H thin films by this surface treatment. In addition to the broad suppression of reflectivity of the treated thin Si films, efficient light-trapping effects approaching the limits predicted by the statistical light trapping theory are observed, increasing the optical path length of light in the thin films by up to 15 μm for films $\sim$1 μm in thickness. These results open an alternative approach to achieving the improved optical performance of thin-film Si solar cells.

II. BLACK ETCHING PROCEDURE AND EXPERIMENTAL DETAILS

Most samples used in this work are prepared via the black etching of a typical a-Si:H film with a nominal thickness of 1.31 μm that is deposited on a flat glass substrate via SiH_4 plasma-enhanced chemical vapor deposition (PECVD). In order to also investigate the optical effects of nanotexture in Si films at the onset of the amorphous-to-crystalline transition, the results for a black-etched 0.73 μm thick μc-Si:H film of low crystalline fraction, deposited via PECVD using a modest hydrogen dilution ($[H_2]/[SiH_4] \approx 25$), are shown as well. Such "on-the-edge" material is of major practical interest, as currently the best microcrystalline solar cells are made of this material.[8,19,20] A more detailed study of black μc-Si in the whole accessible range of crystalline fractions would be of substantial interest, but that is beyond the scope of this work, which is devoted to an exploratory study of the optical effects originating from the black-etching treatment.

Both kinds of black thin films are prepared via the nanotexturing treatment described in more detail in Refs. 17 and 18. In brief, the exposed surfaces of the a-Si:H and μc-Si:H films were processed using the following three-step procedure:

(1) An ultrathin gold layer (1.5 nm by weight-thickness monitor) is deposited first on the flat Si surface via standard thermal vacuum evaporation at a base pressure of 10^{-6} mbar. This layer is discontinuous, consisting of nanometer size Au clusters, and leaves about 30% to 50% of the of Si surface bare, as observed via atomic force microscopy (AFM).
(2) Wet chemical etching in an aqueous solution of HF and H_2O_2 in a volume ratio of HF(50 wt. %):H_2O_2(30 wt. %):$H_2O = 1:5:10$ is carried out at room temperature. The etching process can be visually controlled by observing the surface, which changes gradually from highly reflecting to black. The duration of this step has been varied between 20 and 60 s in order to obtain a series of a-Si:H samples with nanotextures of different depths. The μc-Si:H film has been etched for 45 s only.
(3) The remaining Au is removed via etching in an aqueous solution of iodine and potassium iodide with a weight ratio of I:KI:$H_2O = 1:4:40$ at room temperature for two minutes.

As shown previously,[17] the treatment with these process parameters is driven by Au-catalyzed etching, which is strongly localized close to the metal clusters and, thus, results in the development of a specific nanotexture in the silicon surface as presented in Sec. IV.

The total hemispherical reflection and transmission of the samples were measured at wavelengths between 200 and 2500 nm using a double-beam UV/VIS/IR spectrophotometer equipped with an integrating sphere (Perkin Elmer, Lambda 900). The measurements of weak absorption in the long wavelength spectral region were performed using photothermal deflection spectroscopy (PDS). The paramagnetic defects in the samples were determined from electron spin resonance (ESR) measurements in a Bruker ESP 300 spectrometer at room temperature. The etched surface morphology was investigated via AFM (Veeco, Nanoscope III) and was analyzed using software for the statistical analysis of AFM topography.[21] Aluminum contacts in coplanar geometry, 3 mm wide and separated by a 0.5 mm gap, were evaporated on top of the black-etched samples for dark and photoconductivity measurements. The conductivity measurements were carried out in DC mode using an electrometer (Keithley 617).

III. OPTICAL EFFECTS INDUCED BY THE BLACK ETCHING

A. Photometric spectra

Figure 1(a) presents the effect of the black etching treatment on the total hemispherical reflection of several a-Si:H samples, etched for different durations t_{etch} of step 2. The reflection is measured using illumination through the textured front surface. For clarity, only the portion of the spectra for wavelengths λ between 350 and 1000 nm is shown; this includes the region of strong a-Si:H absorption (photon energies $h\nu$ larger than the bandgap E_g) and the adjacent region of weak sub-band-gap absorption. However, the full spectra, measured up to 2500 nm, were used to obtain the effective (coherent) optical thickness d_{coh} of the a-Si:H layers from the observed interference fringes.[22] Figure 1(a) shows that the major effect of black etching is a dramatic reduction of the surface reflectivity in the entire range of strong a-Si:H absorption (short wavelengths) where the reflection originates from the front surface only, i.e., from the textured film surface. However, the reflection in the sub-band-gap region, where a-Si:H is practically transparent and the overall reflectivity is determined by both, front and rear surfaces, also undergoes a significant modification. After the black etching, the amplitude of the interference fringes in this region diminishes with increasing etching time t_{etch}. This indicates that the interference between the front and the rear film surfaces is destroyed due to the vanishing reflectivity of the front surface and/or because of random scattering of the light crossing the film. For $t_{etch} = 60$ s, the interference fringes vanish completely, prohibiting the determination of d_{coh} via direct optical experiments. For this sample, we estimated a thickness of $\sim$820 nm from extrapolation. Simultaneously, the measured reflectivity becomes determined mainly by the high reflection from the untreated rear a-Si:H/glass surface. It is also evident that the spacing between the interference fringes increases with increasing t_{etch}, showing

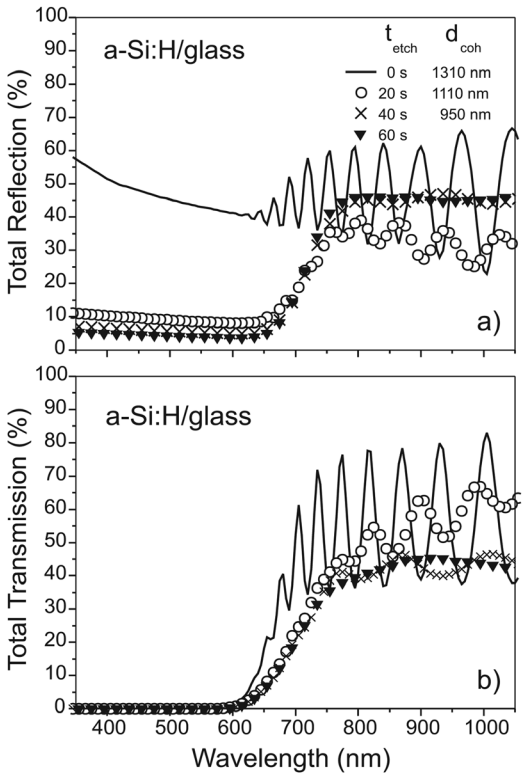

FIG. 1. Photometric spectra of a series of a-Si:H films obtained by black etching for increasing treatment times t_{etch} showing (a) the total hemispherical reflection spectra and (b) the total hemispherical transmission spectra. The respective spectra of the untreated a-Si:H film are indicated by $t_{etch} = 0$ s. The initial thickness of all samples was equal to the thickness of the untreated a-Si:H film; after the etching these samples show the coherent optical thicknesses d_{coh} as indicated.

that the etching causes an effective optical film thickness reduction of about 8 to 11 nm/s. In contrast, changes of the reflectivity cannot be observed at all when the wet chemical etching is performed on a clean a-Si:H surface without prior Au evaporation, even for the longest time, $t_{etch} = 60$ s. Only a very small coherent optical thickness reduction of about 0.02 nm/s can be detected in this case. This clearly shows that the Au clusters have a pronounced catalytic effect on the etching process.

Figure 1(b) shows the total hemispherical transmission of the same set of samples. In addition to the vanishing interference with increasing t_{etch} that has already been discussed, a striking feature of the transmission spectra obtained after black etching is the apparent redshift of the absorption edge as compared to untreated a-Si:H. This tendency is opposite to what is expected for films with decreased overall thickness and is analyzed in more detail below.

The raw reflection and transmission spectra of black-etched microcrystalline silicon films demonstrate the same general features and therefore are not shown here. A particular difference is the optical film thickness reduction with t_{etch}, which is slower for μc-Si:H films ($\sim$2 to 3 nm/s) than for a-Si:H films (8 to 11 nm/s), resulting in a thickness of $\sim$600 nm for the μc-Si:H film after $t_{etch} = 45$ s. As the crystalline phase of "on-the-edge" μc-Si:H films is predominantly found at the top surface,[19,20] we conclude that the amorphous phase is etched faster than the crystalline one. Nevertheless, essentially the same optical effects emerge after the etching.

Figure 2 presents the effect of the black etching treatment on the total optical absorption of the investigated a-Si:H [Fig. 2(a)] and μc-Si:H films [Fig. 2(b)]. The absorption spectra A are obtained from the respective experimental spectra of the total reflection R and the total transmission T by using the fundamental relation $A = 1 - R - T$. The absorption spectra of the untreated samples, after smoothing of the interference fringes via geometrical averaging, and those of the black a-Si:H and μc-Si:H samples with the longest etch duration are shaded for clarity. One can see in Fig. 2 that the overall absorption of the black-etched samples is much higher than that of the untreated films. It is also evident that this increase is a result of two different effects. The increase in the region of strong absorption at short wavelengths (photon energies above the bandgap) obviously originates from suppressed reflection. In addition, an apparent redshift of the absorption edges of all treated samples can be clearly seen. We show in Ref. 17 that there is no additional absorption at crystalline silicon surfaces that were modified by the same black-etching procedure, and this is expected to hold also for thin Si film surfaces. Therefore, we conclude that the red shifts observed here are not associated with added absorption at the film surface itself; instead they should be attributed to an enhancement of the weak near-edge absorption within the silicon thin films. A natural explanation is an increased mean path length of the light rays due to scattering after they enter

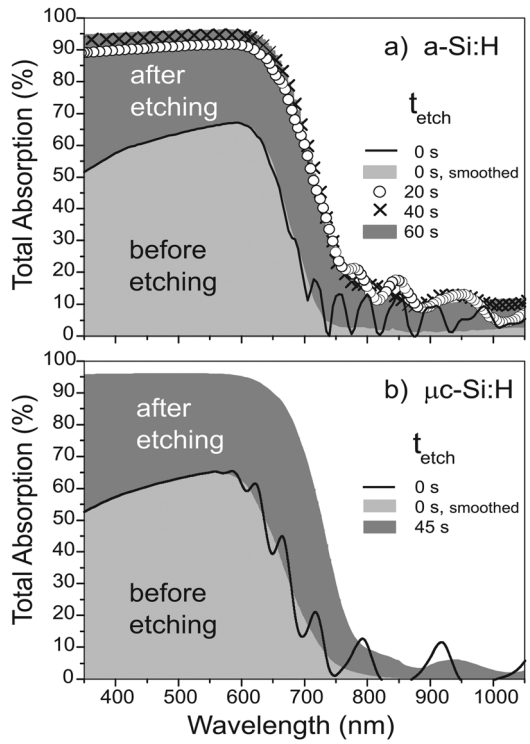

FIG. 2. Total absorption spectra A of (a) the untreated and black-etched a-Si:H films from Fig. 1 and (b) an untreated and black-etched μc-Si:H film. The absorption spectra are calculated from the respective experimental spectra of the total hemispherical reflection R and the total hemispherical transmission T. The spectra of the untreated samples after smoothing of the interference fringes and those of the samples with the longest treatment times are represented by shaded area graphs.

the film through the treated surface, which results in an effective increase of the optical film thickness.

B. Photothermal deflection spectroscopy

The extended absorption spectra of black-etched a-Si:H and μc-Si:H films, in comparison with the corresponding spectra before the black etching, are shown in Figs. 3(a) and 3(b), respectively. The low-absorption parts of these spectra, plotted using symbols, have been obtained via PDS. Because of the homogeneous absorption in this region, the measured PDS signal is proportional to the total absorption A within the film, given by the relation $A = \alpha L$, where α is the absorption coefficient and L is the effective length of the light path within the film. The absorption signals observed via PDS are converted into absolute values by fitting to the photometrically determined spectra obtained in absolute units and shown as lines in Fig. 3. The latter are determined in the region of the fundamental absorption edge, where $\alpha L \approx 1$, by

$$\alpha L = -\ln\left[T/\left(1-R_f\right)\left(1-R_b\right)\right], \quad (1)$$

where T, R_f, and R_b are the spectral values of the total transmission, the total reflection under front illumination (through the air–film interface), and the total reflection under back illumination (through the film–glass interface).

It is important to note that both kinds of measurements determine the overall αL product but do not allow a separation of the individual contributions of the two factors. In general, each of these factors can vary with the wavelength.

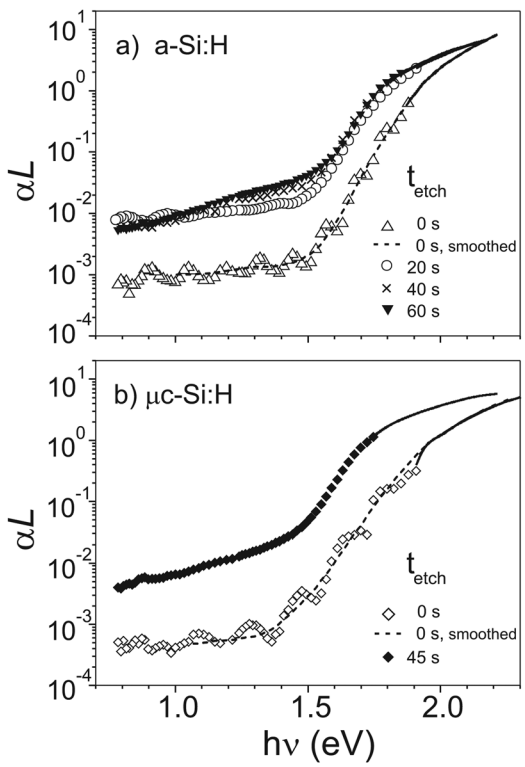

FIG. 3. Extended absorption spectra for (a) the series of untreated and black etched a-Si:H films from Fig. 2(a) and (b) the corresponding μc-Si:H films from Fig. 2(b). The data in the low-absorption region are obtained via photothermal deflection spectroscopy (symbols) and are fitted to the photometrical data (solid lines) in the region where $\alpha L \approx 1$.

Commonly, the absorption coefficient is derived from the αL product by assuming that the length of the light path is the same for all wavelengths and equals the geometrical film thickness. Such an assumption is valid only for a single, straight passage of the light through the thin film, and therefore it is justified only for homogeneous films with flat parallel surfaces[6] (e.g., the films before black etching). However, the assumption will be incorrect in the case of black-etched films because of light scattering at the modified surfaces, which results in prolonged light paths within the films, as is shown below. In particular, the extension of the light path will be dependent on the wavelength.

The absorption spectra of the flat untreated films before the black etching ($t_{etch} = 0$) can be interpreted as usual to represent the spectral dependence of the absorption coefficient of the as-grown a-Si:H and μc-Si:H materials, which we denote by α_0. Thus, for these thin films, α_0 multiplied by constant factors equal to the respective film thicknesses (1.31×10^{-4} cm for the a-Si:H film and 0.73×10^{-4} cm for the μc-Si:H film) is plotted in Fig. 3. One can see that both kinds of untreated materials exhibit quite similar absorption coefficients because of the low crystalline fraction of the investigated μc-Si:H sample. Slightly different Urbach tail widths of ~59 meV and ~78 meV for a-Si:H and μc-Si:H, respectively, can be determined from the linear parts of the spectra in the semi-logarithmic plots. The higher value for the μc-Si:H sample can be attributed to the coexistence of amorphous and crystalline phases in it. The defect related absorption α_0 at $E_g \leq 1.3$ eV of both untreated (flat) samples levels out at $\alpha_0 \approx 10^1$ cm^{-1}, indicating that the PDS measurements have been partially affected by additional glass substrate absorption at long wavelengths,[23] which was not avoided in our experiment. This assumption is supported by ESR measurements of the untreated (flat) a-Si:H samples, which show dangling bond densities of about 10^{16} cm^{-3}, corresponding to an optical absorption coefficient at 1.3 eV of $\alpha_0 \approx 10^0$ cm^{-1}.[24]

A remarkable alteration of the absorption develops after the black etching treatment of a-Si:H films, as can be seen in Fig. 3(a). The absorption αL in the entire region between 0.8 eV and 2.2 eV is considerably enhanced even after the shortest etching duration of 20 s. A longer etching duration results in a further absorption enhancement, saturating at $\tau_{etch} \sim 40$ to 60 s. Simultaneously, only a minor increase of the Urbach tail width of all treated a-Si:H samples is observed (from 59 to 64 ± 3 meV). The absorption enhancement caused by the black etching is even more pronounced in the μc-Si:H sample shown in Fig. 3(b). Surprisingly, the Urbach tail width of the black μc-Si:H (67 meV) is less than that of the untreated μc-Si:H (78 meV).

Usually, the enlarged absorption at $h\nu \leq 1.3$ eV in a-Si:H-based films is attributed to an increased density of dangling bond defects in the material. Such an explanation does not seem appropriate for the black-etched samples shown in Fig. 3 because of the concomitant absorption enhancement at higher photon energies of up to 2.2 eV. In the case of absorption changes caused by defects, only absorption in the spectral region below 1.3 eV is enhanced. Furthermore, ESR measurements show only a small increase

of the dangling bond density in the black-etched samples by factors of 3 to 6, which correlates with their enlarged surface area. Expressed as a volume density, the ESR dangling bond concentration remains below 10^{17} cm^{-3} for all samples in Fig. 3(a). This value corresponds to a defect-related absorption index $\alpha(1.3\ \text{eV}) \approx 10^{1}$ cm^{-1},[24] which is much too low to account for the high optical absorption observed at 1.3 eV, which, if originating from dangling bonds, would correspond to dangling bond densities exceeding 10^{18} cm^{-3}.[24] Similarly, the strong photoconductivity of the samples discussed in Sec. V is at variance with the idea of such large concentrations of defects being the reason for the absorption enhancement. Thus, a purely defect-related origin of the observed broad absorption enhancement can be ruled out. However, such an enhancement can be naturally explained by the effects of light trapping leading to an effective increase of the path length L, as discussed below.

C. Analysis of the light trapping effect

The theory of statistical light trapping[10,11] describes the case in which the light paths within an absorbing film are randomized by intensive scattering and subsequent total internal reflection at the film surfaces. To demonstrate the consistency of the experimentally observed absorption enhancement in our black-etched samples with this theory, we analyze the experimental data from Fig. 3 following the procedure used by Deckman, Roxlo, and Yablonovitch.[11] The experimentally obtained αL products of all samples were used directly, without separation of the factors, to calculate the spectra of the internal absorption probability A_p according to

$$A_p = 1 - \exp(-\alpha L). \tag{2}$$

A_p is independent of the surface reflectivity (only light propagation within the film is considered) and thus represents only the light trapping effects due to the differences in the effective αL products. The A_p spectra of the untreated (flat) a-Si:H film and those of black a-Si:H samples after etching for different durations are presented in Fig. 4(a). The corresponding A_p spectra of μc-Si:H films before and after black etching are presented in Fig. 4(b). The same figures also show the theoretical curves for the maximally enhanced absorption A_{max}, which can be achieved via the total randomization of the light paths within the film. These curves were obtained using the relation

$$A_{max} = \{1 - \exp(-2\alpha_0 d_{coh})\}/\{1 - \exp(-2\alpha_0 d_{coh}) + (n_0/n)^2 \tau_f \exp(-2\alpha_0 d_{coh})\} \tag{3}$$

given by statistical light-trapping theory.[11] Here d_{coh} is the film thickness, obtained from the interference fringes as described in Sec. III A. Again, α_0 is the absorption coefficient of the a-Si:H or μc-Si:H material as obtained from the experimental data for the untreated samples with $\alpha L = \alpha_0 d_0$. The α_0 spectra for the untreated samples used for the calculation have been smoothed by geometrical averaging in order to remove the interference fringes prior to the calculation of A_{max}. Furthermore, n is the refractive index of a-Si:H or

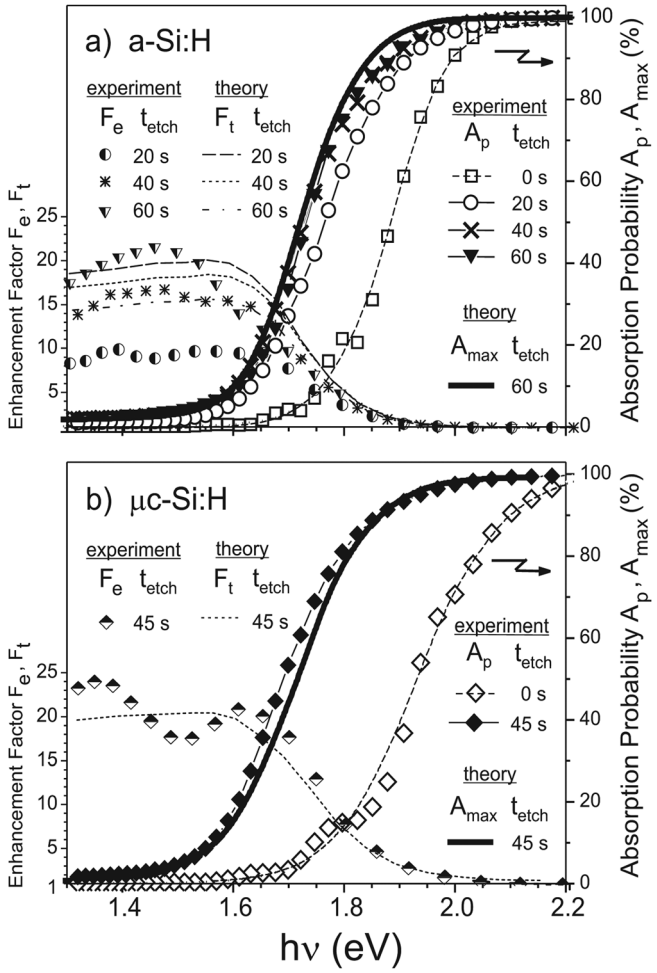

FIG. 4. Enhancement of the internal absorption probability due to light trapping in the black-etched (a) a-Si:H and (b) μc-Si:H films from the previous figures. The spectra A_p, represented by symbols, are obtained directly from the experimental data and are linked to the right-hand scale. The solid curves A_{max} represent the spectra of the maximally achievable absorption in the films investigated according to the theory of statistical light trapping. The experimentally obtained absorption enhancement factors F_e are represented as indicated in the left-hand legend and are linked to the left-hand scale. The respective theoretical enhancement factors F_t are represented by broken lines.

μc-Si:H obtained from the photometric transmission spectra of the untreated film, n_0 is the refractive index of the medium surrounding the thin film (which in our PDS measurements is perfluorohexane, with $n_0 = 1.25$), and τ_f is the Fresnel transmission coefficient of the ideally flat film–substrate interface (calculated as $\tau_f = 4n_g n/(n_g + n)^2$, where $n_g = 1.48$ is the refractive index of glass substrate). A_{max} represents the internal absorption probability in the case of full statistical light trapping when the weakly absorbed light propagates inside the film along various paths with equal probabilities in all directions (totally randomized light paths) but can leave the film only through narrow escape cones limited by the total internal reflection of the film surfaces ($\sim \pm 14°$ from the normal for the Si–air interface and $\sim \pm 22°$ for the Si–glass interface).

Figure 4 clearly demonstrates a greatly enhanced absorption probability in the black-etched a-Si:H and μc-Si:H films. For a-Si:H [Fig. 4(a)], a short etching ($\tau_{etch} = 20$ s) results in a significant shift of the experimentally

obtained A_p toward the theoretical A_{max}, but it doesn't reach it. For comparison, note that the antireflection effect of the black surface is almost completely established already at this etching duration [see Figure 1(a)]. This indicates that the light trapping and the reduction of reflectivity in our samples might have correlated, but not identical, origins. With longer etching durations, the experimental A_p values are further enhanced and tend to stabilize for $t_{etch} > 40$ s, reaching the theoretical limit of full light trapping. Moreover, the agreement between experiment and theory holds in the whole investigated spectral range, which validates that the observed absorption enhancement originates from light trapping effects and not from an alteration of the absorption coefficient. Similarly, the experimental enhancement of A_p in the black μc-Si:H sample treated for 45 s, shown in Fig. 4(b), reaches the theoretical limit within error margins.

Figure 4 also shows the variation of the absorption enhancement factors F for the black-etched films with respect to the untreated (flat) samples, as calculated by

$$F_e = A_p(black)/A_p(untreated) \tag{4}$$

for the experimentally observed absorption and by

$$F_t = A_{max}/A_p(untreated) \tag{5}$$

for the theoretically expected enhancement. The maximum value that these factors can approach depends on the refractive indices of the surrounding dielectric medium n_0 and the film material n according to the relation $F_t = 2(n/n_0)^2$ (or $4(n/no)^2$ with an additional back reflector).[11] As the PDS measurements were carried out in perfluorohexane ($n_0 = 1.25$), the F_e and F_t factors reach maximal values of ~20, whereas with air as the surrounding medium they should be as high as ~25. These large numbers are reached at photon energies $h\nu < 1.6$ eV, where the absorption coefficient of a-Si:H is low ($\alpha_0 \leq 10^2$ cm^{-1}). From the viewpoint of its application in thin-film Si solar cells with typical thicknesses of ~1 μm, the absorption enhancement via black etching in the range of $\alpha_0 \approx 10^2$ to 10^3 cm^{-1} (the beginning of the absorption edge), corresponding to photon energies between 1.65 and 1.75 eV, is of major importance. Whereas the total internal absorption probability of untreated a-Si:H or μc-Si:H films with a thickness of ~1 μm in this energy region is below 5%, the absorption probability of the black-etched samples in the same range is enhanced by factors of 8 to 15 to useful levels of 20% to 60% for the a-Si:H films [Fig. 4(a)] and 30% to 70% for the μc-Si:H sample [Fig. 4(b)], despite the 200 to 300 nm reduction of the physical film thickness caused by the etching. This light trapping effect leads to an expansion of the usable absorption range of the black-etched Si films toward the infrared region. The expansion amounts to about 0.2 eV, corresponding to a redshift from ~630 nm to ~730 nm of the effective absorption in the samples investigated here. An even more pronounced spectral expansion of the absorption after black etching can be expected for highly crystalline μc-Si:H (or polycrystalline Si) films, because the true absorption coefficient of the crystalline Si phase, in contrast with that of the amorphous one, remains in the range of $\alpha_0 \approx 10^2$ to 10^3 cm^{-1}, which is favorable for complete light trapping in films with a physical thickness of ~1 μm, down to photon energies as low as $h\nu \approx$ 1.3 eV ($\lambda \approx 950$ nm).[6]

IV. SURFACE MORPHOLOGY: ORIGIN OF THE OPTICAL EFFECTS

The origin of the optical effects induced by the black etching can be understood from the morphology of the surfaces shown in Fig. 5. Figures 5(a)–5(c) present 3D AFM images of three a-Si:H surfaces, obtained after various

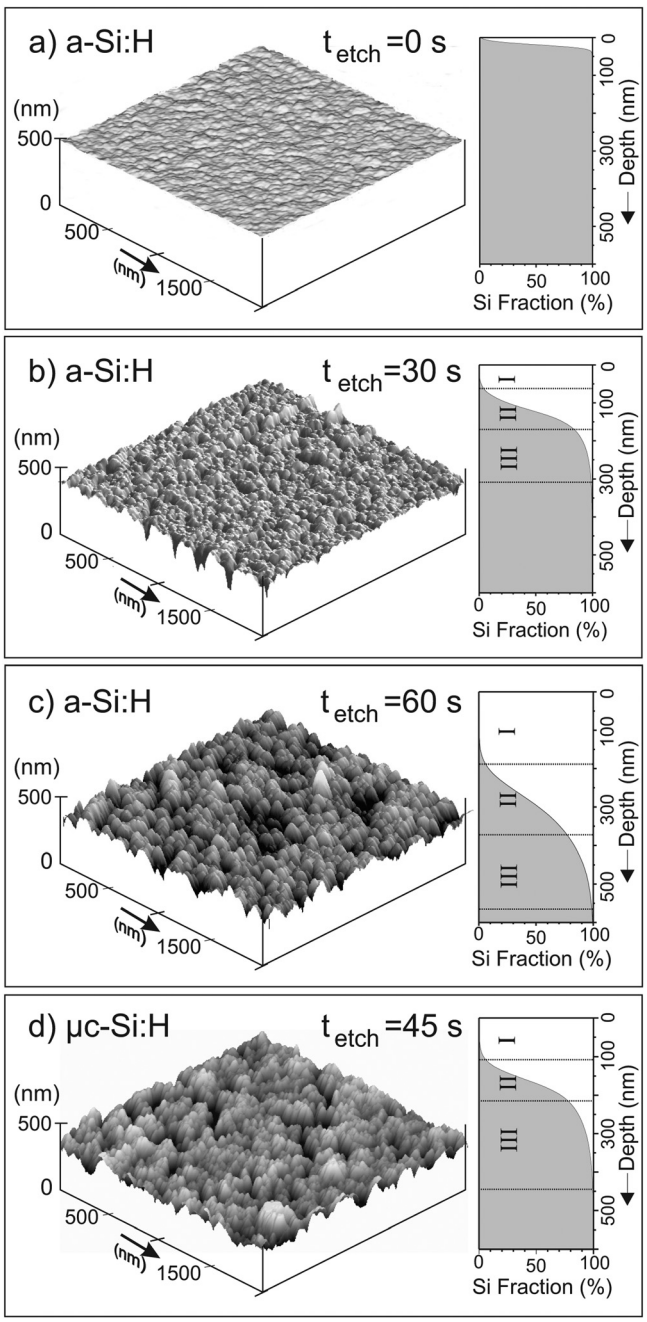

FIG. 5. Three-dimensional atomic force microscopy images of (a) an untreated a-Si:H surface, (b),(c) a black-etched a-Si:H surfaces with increasing treatment time t_{etch}, and (d) a black-etched µc-Si:H surface. The variation of the silicon fraction at the air–Si interface of the films as obtained via statistical analysis of the AFM data is shown in the diagram at the right-hand side of each image.

durations of the wet etching. The vertical scale is the same in all images and equals the horizontal scale. Thus, the images depict the actual unscaled morphology of each surface. The diagrams at the right hand side of each image illustrate the variation of the silicon fraction across the textured layer of the respective film. They are obtained through the integration and normalization of the height histograms of the AFM images.[21] The silicon fraction at a certain depth is defined as the integrated cross-sectional area of all protruding Si features that are traversed by a horizontal plane, normalized to the whole lateral image area (2×2 μm^2). The complement presents the fraction of the surrounding medium (e.g., air). The depths of the traversing planes are measured from a horizontal zero plane parallel to the substrate, which is chosen to touch the highest point of the respective AFM image presumably remaining from the initial non-etched surface. The Si fraction diagrams present only the topmost transient regions of the films, though each of the investigated films has at least a 500 nm thick dense Si bulk lying below it.

The image in Fig. 5(a) shows an untreated a-Si:H surface ($t_{etch} = 0$ s). One can see that such a surface is naturally rough on a very fine scale. Convex features with characteristic lateral sizes δ of 50 to 150 nm—much smaller than the wavelengths of the light from the relevant part of the solar spectrum—can be distinguished in the image. The respective Si fraction diagram shows that these features penetrate less than 30 to 40 nm into the a-Si:H film, so that the transition from the surrounding medium to the silicon takes place over a distance that is much smaller than the wavelengths of the light in the whole spectral range of interest. Such a surface can be described as optically flat. It should have a high mirrorlike reflectivity that is determined by the Fresnel reflection coefficient, as experimentally observed in Sec. III A.

The AFM images of the black-etched a-Si:H surfaces [Figs. 5(b) and 5(c)] reveal a rather different morphology. One can see in Fig. 5(b) that even a short etching ($t_{etch} = 30$ s) results in a pronounced surface texture. The major part of this texture consists of densely packed sharp silicon hillocks with lateral sizes δ in the same 50-150 nm range. The key difference relative to the features on the untreated a-Si:H surface is that these hillocks are significantly higher, i.e., they penetrate much deeper into the silicon film. With increasing black etching duration [Fig. 5(c), $\tau_{etch} = 60$ s], the hillocks become more pronounced, with considerably increased penetration depths but slightly enlarged lateral sizes δ of 80 to 170 nm. The corresponding Si fraction diagrams show that the transition region between the surrounding medium and silicon is greatly extended and can be virtually divided into three layers (I, II, and III) below the zero plane. The topmost layer (I) is characterized by a vanishingly small Si fraction because it contains only the tips of a few very high peaks approaching the zero plane, and almost the entire silicon material is etched away. Thus the actual Si surface appears to be shifted below the zero plane (at the onset of region II). The next layer (II) is characterized by an almost linear increase of the silicon fraction with depth. Such a dependence corresponds to a transition across the major structural features of the texture, from the top of the cone-like Si hillocks to their bottom. From an optical point of view, this layer can be represented by an effective optical medium, because the hillocks are not distinguishable from the surrounding medium by light with effective wavelengths $\lambda_{eff} = \lambda_{air}/n_{Si}$ higher than $\delta \sim 100$ nm, which corresponds to $\lambda_{air} > 400$ nm. Therefore, the Si fraction diagram shows that layer II is an effective medium with smoothly (almost linear) varying optical density that can be described by the model of Stephens and Cody.[25] This model predicts that the reflectivity of such a gradual boundary layer is vanishing for wavelengths below a cut-off threshold that depends on the refractive index of the bulk material, as well as on the depth of the textured layer. Accordingly, the reflectivity cut-off for finely textured silicon surfaces with a linearly increasing density should appear at a wavelength that is about 6 times larger than the depth of the graded density layer (see Table 1 in Ref. 25). Thus, the graded Si-density layer II in Figs. 5(b) and 5(c) (depths of ~130 nm and ~180 nm, respectively) should result in a strong suppression of the reflection from the corresponding surfaces for light wavelengths shorter than ~780 to 1100 nm, i.e., in the whole usable absorption spectra of a-Si:H and μc-Si:H films. This fully explains the experimentally observed antireflection properties of the black-etched silicon films presented above.

The third layer, III, which is characterized by a slower increase of the Si density, can also be distinguished in the Si fraction diagrams of Figs. 5(b) and 5(c). An inspection of the AFM image in Fig. 5(b) reveals that this layer contains several sharp and deep pits, starting from the apparent surface with orifices ~150 to 250 nm in diameter and reaching maximum depths of ~250 nm. These pits are separated laterally by distances on the order of 350 to 700 nm as far as can be observed in the limited image area. With increasing etching duration [Fig. 5(c)], the sharp pits develop into broader valleys with finely textured inner surfaces. They are similarly spaced (350 to 700 nm) but have larger diameters and depths (~300 to 400 nm). The depth/diameter aspect ratio is close to 1 for both the initial pits and the developed valleys. We assume that such secondary texture features can be the reason for efficient diffractive light scattering, as their dimensions and, especially, spacing are comparable to the wavelengths of light from the visible and near infrared ranges. Such scattering should result in light trapping within the underlying silicon film as discussed in Sec. III C.

An estimation of the conditions for efficient light trapping can be made using the following rather general considerations. If we imagine a virtual transmission dot diffraction grid on top of the film with an average distance Δ between scatterers, the directions of constructively interfering rays after passing the grid should be given by Bragg's equation, $\lambda_{air}/n_{Si} = \Delta \sin(\gamma)$, where λ_{air} is the wavelength of the incident light in the surrounding medium (e.g., air) and λ_{air}/n_{Si} and γ are the effective light wavelength and the scattering angle within the Si film, respectively. Furthermore, we consider that efficient light trapping occurs for rays that enter the film (scattering angles $\gamma < \pi/2$ with respect to the direction of the incident beam) and reach the rear film–glass interface under angles γ higher than the critical one for total internal reflection. These assumptions are equivalent to the requirements $0 < \sin(\gamma) < 1$ and $\sin(\gamma) > 1/n_{Si}$. Applying

these inequalities to Bragg's equation gives the overall requirement

$$\lambda_{air}/n_{Si} < \Delta < \lambda_{air} \quad (6)$$

for the average distance between the scattering centers that can induce efficient light trapping via diffractive scattering. The light absorption enhancement, which can be beneficial for a thin film, should occur at light wavelengths longer than the absorption edge of the film, i.e., for typical Si films with a thickness of ~1 μm in the range of $\lambda_{air} \approx$ 700-1000 nm. Thus, favorable distances between the scattering features on the surface of such films ($n_{si} \approx 3.5$) should be in the range of ~200 nm $< \Delta <$ 1000 nm according to Eq. (6). Larger as well as smaller spacings (e.g., the small hillocks in the primary texture) will be inefficient for light trapping by diffractive scattering. As described above, the spacing between the secondary features of the black-etched silicon films (pits and valleys spaced at 350 to 700 nm) match perfectly the favorable range. Such spacing results in rather high scattering angles (above the critical angle) that considerably prolong the light paths, accounting for the near-perfect light trapping effects observed in the black-etched a-Si:H films.

Figure 5(d) shows the surface morphology of the black μc-Si:H sample. A primary texture of densely packed silicon hillocks with lateral sizes δ in the 50-150 nm range, quite similar to the the a-Si:H sample from Fig. 5(b), can be seen in Fig. 5(d). This kind of texture is responsible for the antireflection properties of the black-etched μc-Si:H surface in the same way as for the black a-Si:H surface. However, an inspection of Fig. 6, which shows the 2D AFM images of the a-Si:H and μc-Si:H surfaces from Figs. 5(c) and 5(d), respectively, reveals the presence of a secondary texture with a different character. Instead of the broad valleys dispersed on the a-Si:H film surface [Figs. 5(c) and 6(a)], a net of sharp canyons and pits is found on the otherwise flatter μc-Si:H surface [Figs. 5(d) and 6(b)]. One can speculate that such features originate from the faster etching of the amorphous fraction in the μc-Si:H film mentioned in Sec. III A. The lateral distances between the deep features in Fig. 6(b) are broadly distributed in the 200-800 nm range, even better fitting the range of distances between scattering features that favor efficient light-trapping. The differences in the AFM images are demonstrated more clearly in the respective Si fraction diagrams. Layers II and III, associated with the primary and secondary texture, respectively, have nearly equal depths in the diagram of the a-Si:H film. In contrast, these regions in the μc-Si:H film are more distinct with a greater depth of layer III. We assume that such a pronounced secondary texture causes a more intensive diffractive scattering of the light entering the film, and this might be the reason for the full light-trapping effect observed in the μc-Si:H sample. It would therefore be interesting to study the effects of black etching on the structural and optical properties of μc-Si:H in more detail, in particular as a function of the crystallinity of the films.

Finally, we would like to emphasize that the surface morphology of the black-etched films differs substantially from that of porous Si, which has been observed by other authors using metal-catalyzed etching of silicon.[26]

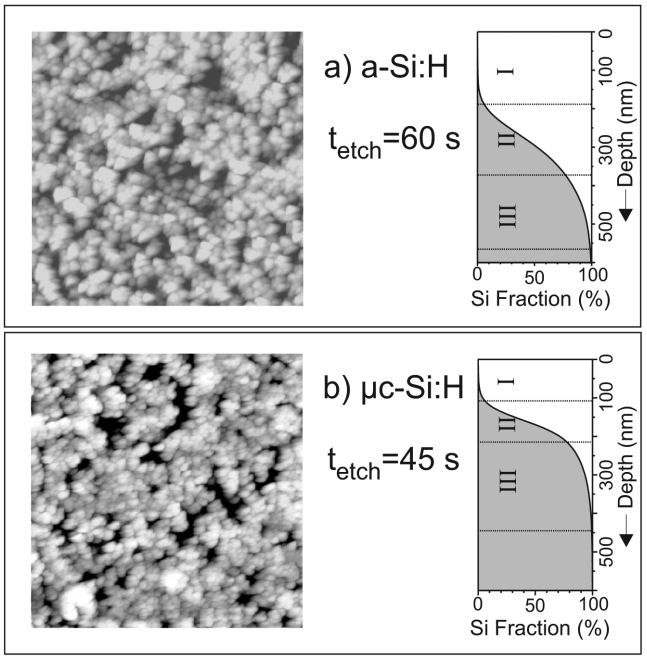

FIG. 6. Two-dimensional AFM images (a) of the black-etched a-Si:H sample from Fig. 5(c) and (b) of the black-etched µc-Si:H sample from Fig. 5(d).

V. PHOTOCONDUCTIVITY

A. Spectral measurements in coplanar contact geometry

Figure 7 shows the photoconductivity spectra σ_{ph} of black-etched a-Si:H samples with different t_{etch} in comparison with the spectrum of an untreated a-Si:H film. All spectra were measured in coplanar contact geometry (with a conductive gap 0.5 mm long and 3 mm wide) and have been normalized to a constant illumination power density assuming monomolecular recombination[27] for the low photocarrier generation rate in our experiment, which was carried out at illumination power densities below 1 mW/cm^2.

Figure 7(a) presents the spectra obtained via illumination of the front (a-Si:H surface) side of the samples. A comparison of Fig. 7(a) with Fig. 2(a) reveals that the photoconductivity spectrum of the untreated a-Si:H film follows the shape of the respective optical absorption spectrum in the whole investigated spectral region, whereas the spectra of the black-etched films differ considerably. In particular, the photoconductivity spectra of the black-etched films seem to shift toward longer wavelengths with increasing t_{etch} when compared with the spectrum of the untreated film. The long-wavelength shoulders of the photoconductivity spectra for the black-etched samples quite precisely trace the respective shifts of the optical absorption edges of these samples, as can be seen by comparing Fig. 7(a) and Fig. 2(a). This shift is in very good agreement with the spectral expansion of the optical absorption due to the light trapping already discussed. The light trapping dominantly concerns the weakly absorbed (i.e., deeply penetrating) light, and thus the effect takes place in the bulk of the treated films below the textured layer. Thus the excess carriers generated by the trapped light reside in the bulk, where they can drift freely

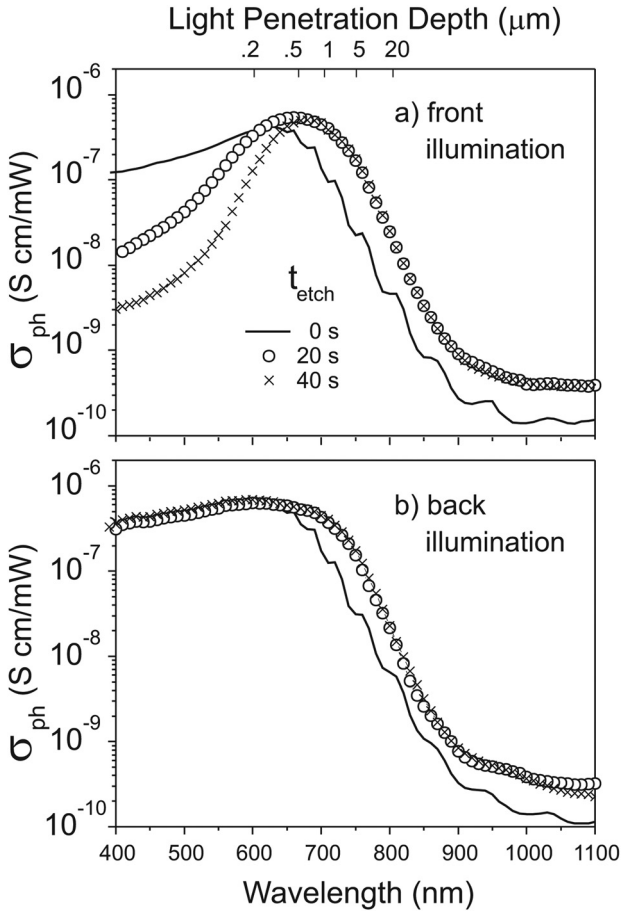

FIG. 7. Photoconductivity spectra σ_{ph} of a-Si:H films treated by black etching with increasing treatment t_{etch} (a) under illumination of the air-exposed black-etched side of the films and (b) under illumination of the films through the glass substrate.

along the electric field between the two laterally spaced contacts. Therefore, the long wavelength shoulder of the photocurrent under front illumination correlates closely with the optical absorption and can be attributed to an increased photogeneration of excess carriers due to light trapping. In contrast, the photocurrent observed under front illumination with short wavelengths shows a sharp cutoff in spite of the high optical absorption due to the reduced reflectivity in this spectral region. We show in Sec. IV that the depth of textured layers II and III of the black-etched films increases with the etching duration (from ~220 nm for $t_{etch} = 20$ s to ~350 nm for $t_{etch} = 40$ s). A comparison with the light penetration depth scale at the top of Fig. 7(a) [the penetration depth is defined as $1/\alpha_0$, where α_0 is taken from Fig. 3(a)] reveals that the photocurrent cutoff in each black sample occurs in a wavelength range that corresponds to light absorption within the respective textured layer. Because the diffusion length of the excess carriers in a-Si:H-based materials is very small, the carriers that are photo-generated within the separated hillocks of the nano-texture by strongly absorbed (short wavelength) light cannot diffuse to the underlying continuous film. Thus they can contribute to a current between the coplanar contacts via merely a few percolation paths, which are vanishing toward the film surface. Therefore, the photoconductivity cutoff at short wavelengths (shallow light penetration) can be explained by geometrical reasons rather than by the enhanced recombination of charge carriers in the modified films. Consequently, the photocurrent suppression at short wavelengths observed here is an artifact of the coplanar contact measurement and should not be expected in black silicon films or devices that operate in sandwich contact configuration, e.g., solar cells.

Figure 7(b) shows the photoconductivity spectra of the same samples when the absorbing films are illuminated through the transparent glass substrate, i.e., from the back, untreated side of the samples. In contrast to Fig. 7(a), all spectra in Fig. 7(b) merge at short wavelengths (strongly absorbed light), as can be expected, because the glass–a-Si:H interfaces of all samples are identical. The long wavelength shoulders of the back-illumination spectra again exhibit a redshift of the absorption edge for the black-etched samples, similar to the spectra shown in Fig. 7(a). Obviously, the highly penetrating light from this spectral region reaches the textured front surface, and the observed redshift implies intensive light back scattering, which is not observed (as reflectivity) under front illumination of these surfaces. The origin of such an asymmetry could be related to the fact that the light propagating in silicon has much shorter wavelengths than that in air due to the high Si refractive index. Thus, the features of the surface texture are effectively larger for the light approaching from the silicon side than that coming from the air side. As a result, the smallest features of the nanotexture are distinguishable as scatterers from the Si side, whereas they are accepted as an effective medium with a gradually changing refractive index (black surface) when approached from the air side. This phenomenon might be very useful in thin-film solar cells in a superstrate configuration.

B. Stripe illumination experiment

Further, we employed a modification of the coplanar-contact photocurrent measurement technique in order to directly observe the internal light scattering in the black silicon films. This modification is referred to here as the "stripe illumination experiment." The principle of the experiment is illustrated in the inset of Fig. 8. In the experiment, two photocurrent spectra of the same sample are measured consecutively under different illumination conditions. The first wavelength scan is performed as usual via full illumination of the whole gap between the coplanar contacts ($[0.5 \times 3]$ mm^2 in our experiment) by a light stripe that is parallel to the gap and broad enough to cover it completely. The second scan is made after rotating the sample by 90°, so that the illuminated stripe is perpendicular to the contact gap. The stripe is then adjusted to the smallest possible width (about 0.03 mm in our experiment), and the second photocurrent spectrum is measured under these conditions. After completing the measurements, the ratio of the currents obtained in the second and first scans is calculated. Such a current-ratio spectrum should depend only on the geometrical ratio of the photoconducting stripe widths in the two illumination scenarios, and thus it should be constant as a function of the light wavelength ($\sim 0.03/3 = 0.01$ in our experiment) for a film in which the light does not scatter below the illuminated surface, i.e., where the conducting path width is the same as that of the illumination stripe.

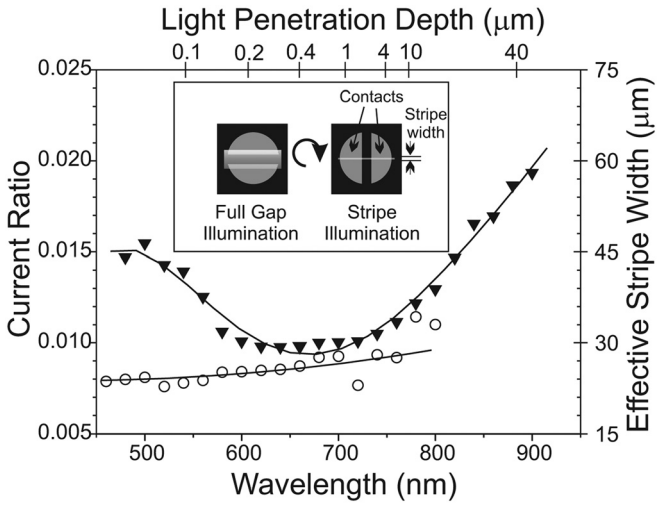

FIG. 8. Stripe illumination experiments carried out with a a-Si:H thin film before (open circles) and after (black triangles) black etching. The principle of the experiment is illustrated in the inset. The lines are guides for the eye only.

Figure 8 presents the current-ratio spectrum of a black etched a-Si:H film ($t_{etch} = 40$ s) compared to that of an untreated a-Si:H film. The vertical scales in the figure are correlated, and the right-hand one shows the effective photoconducting stripe widths that correspond to the current ratios in the left-hand one. One can see that the ratio spectrum of the untreated (flat) film almost does not change with the wavelength, remaining close to a ratio of 0.01, as expected for a fixed illumination stripe geometry. This tendency cannot be well confirmed at wavelengths longer than ~750 nm because the photocurrent measurements of the untreated a-Si:H become unreliable in this region due to a low signal-to-noise ratio caused by the vanishing optical absorption of the flat film. In contrast, the spectrum of the black a-Si:H thin film indicates a well pronounced variation of the effective photoconducting stripe with the wavelength. A flat region, related to an unchanged effective stripe width, can be observed in this sample only in the wavelength range of $\lambda \approx$ 600–720 nm. This range corresponds to light penetrating ~0.2 to ~1 μm into the film (see the top scale). This is the light that is transmitted through the textured layer but absorbed in the film during a single pass. In contrast, the light of longer and of shorter wavelengths broadens the effective photo-conducting stripe, as indicated by the increasing photocurrent ratios there. The increased photocurrent ratio at wavelengths longer than 750 nm corresponds to the weakly absorbed light that can penetrate silicon for large distances before absorption. The associated broadening of the effective photocurrent collection stripe (from ~30 μm to ~60 μm) in this region shows that most of the light actually travels significant distances laterally (~15 μm from the stripe edge) in the black-etched film that is only about 1 μm thick—i.e., it remains trapped in the film where it is absorbed. Thus, the increase of the photocurrent ratio at long wavelengths is in fact a direct observation of a prolonged absorption light path resulting from the black-etching treatment of the film surface. The observed effect is equivalent to an increase of the optical thickness of the film by a factor larger than 10, in good agreement with the analysis of light trapping effects made in Sec. III C.

The short wavelength broadening of the effective photocurrent collection stripe corresponds to light that is absorbed completely within the textured layer (see the top scale of the figure). Such a broadening can be explained if one considers that a part of the light is scattered at surface glazing angles when entering the film and thus can reach the tops of the hillocks that are outside of the stripe where it can be absorbed. Therefore, the short wavelength increase of the current ratio (not the currents themselves) can be associated with an external spreading of the illumination stripe.

VI. POSSIBLE APPLICATION IN SOLAR CELLS

The beneficial optical effects described in this study could be employed in thin film Si solar cells with minimal alteration of the established technology using the following approach: First, a typical n-i (or p-i) structure of a-Si:H or μc-Si:H layers with an overall thickness of ~0.5 to 1 μm is deposited. Then the surface of the topmost intrinsic Si layer is black etched in order to obtain the optically active nanotexture. Subsequently, an ultrathin p- (or n-) doped layer with a thickness of ~20 to 50 nm is conformally deposited over the textured surface to form a complete n-i-p (or p-i-n) cell. In that way the top surface of the cell repeats the nanotexture established by the black etching. Such an approach is most suitable for application in thin-film solar cells built on flexible but opaque substrates (e.g., metal foils) because their illuminated surface is exposed for the black etching treatment. Presently, however, such cells have lower efficiencies than the cells built on transparent textured substrates (superstrate configuration), mainly because of the lack of efficient light-trapping schemes and high reflectivity of the top Si film surface. Nanotexturing of this surface can substantially improve the optical absorption in the underlying active i-layer, thus resulting in higher short circuit currents (respectively increased efficiencies) of the cells in the substrate configuration. Hence, a significant improvement of the performance/cost ratio of black-etched thin film Si solar cells can be anticipated.

The black etching treatment can also be very beneficial for solar cells utilizing μc-Si:H or poly-Si thin films as a light absorber. The growth of thick enough films of these materials (thickness $\geq$ 3 μm), which is needed in order to fully utilize the broader, but overall weaker, absorption of the crystalline Si phase, encounters technological problems at present. On the other hand, we demonstrate here that black etching of such films with physical thicknesses of ~1 μm results in the effective enlargement of the optical thickness to >10 μm and a considerable broadening of the usable spectrum down to ~1.3 eV. Thus, black-etched μc-Si:H or poly-Si thin films can be excellent broad-band absorbers for thin-film solar cells.

Similar approaches are applicable to tandem or micromorph solar cells. In this case, a complete n-i-p a-Si:H cell (instead of a single doped layer) is grown conformally on the top of an underlying nano-textured cell in a substrate configuration. The optical effects of the nanotexture allow this top cell to be extremely thin ($\leq$100 nm) and thus resistant to light-induced degradation, without losing the ability to

absorb most of the blue-green portion of the solar light. Simultaneously, the randomized light paths allow enhanced absorption of the red and near-infrared portions of the spectrum within a reasonably thick bottom cell.

VII. CONCLUSIONS

The metal-catalyzed black-etching treatment applied to thin a-Si:H and μc-Si:H films results in a significant improvement of the optical properties of the films via (i) a nearly complete suppression of the surface reflectivity in the entire region of useful optical absorption and (ii) an efficient light trapping that manifests itself in a broadening of the absorption toward the infrared spectral region. The typical net effect is a doubling of the total optical absorption of the treated films, despite their slightly decreased geometrical thickness.

The observed optical effects are attributed to the formation of a nanoscale texture on the treated surface, which normally occupies only the topmost 200 to 300 nm of the film. This texture has a specific morphology that leads to a smooth transition of the refractive index from that of air to that of Si, thus resulting in reduced surface reflection with a concomitant improvement of the light coupling to the film bulk. Simultaneously, the light propagation is randomized by scattering after crossing the textured surface, which results in efficient light trapping in the film. The analysis of the absorption enhancement at long wavelengths shows that the efficiency of the light trapping induced by the black etching reaches the theoretical limits.

Photocurrent measurements using a coplanar contact configuration show an increase of the photocurrent in the long wavelength range that corresponds to the enhanced optical absorption of the films there. A quantitative stripe illumination measurement reveals a prolongation of the light absorption path in this spectral region that is equivalent to a more than tenfold increase of the effective optical thickness of black-etched films with a physical thickness of $\sim$1 μm, in full agreement with the optical analysis.

The improvement of the optical performance of a-Si:H and μc-Si:H films induced by the black etching treatment could be important for their application in a new generation of thin film solar cells. Possible cell designs that could benefit from a nanotextured surface were discussed.

ACKNOWLEDGMENTS

The authors gratefully acknowledge collaboration with S. Klein, who provided the a-Si:H and μc-Si:H samples. The ESR experiments were performed by S. Niesar. This work was partially supported by the EU via project NanoPV (FP7-NMP3-SL-2011-246331).

[1]W. Kuhler, Appl. Phys. A **53**, 54 (1991).
[2]G. Yue, B. Yan, J. Yang, and S. Guha, Appl. Phys. Lett. **86**, 092103 (2005).
[3]G. Beaucarne, Adv. OptoElectron. 2007, Article ID 36970, 12 pages, (2007).
[4]J. Meier, R. Fluckiger, H. Keppner, and A. Shah, Appl. Phys. Lett. **65**, 860 (1994).
[5]J. Meier, S. Dubail, J. Cuperus, U. Kroll, P. Torres, J. A. A. Selvan, P. Pernet, N. Beck, N. Pellaton Vaucher, Ch. Hof, D. Fischer, H. Keppner, and A. Shah, J. Non-Cryst. Solids **227–230**, 1250 (1998).
[6]M. Vanecek, A. Poruba, Z. Remes, N. Beck, and M. Nesladek, J. Non-Cryst. Solids **227–230**, 967 (1998).
[7]S. Klein, J. Wolff, F. Finger, R. Carius, H. Wagner, and M. Stutzmann, Jpn. J. Appl. Phys. Vol. **41**, L10 (2002).
[8]S. Klein, F. Finger, R. Carius, and M. Stutzmann, J. Appl. Phys. **98**, 024905 (2005).
[9]K. Yamamoto, M. Yoshimi, Y. Tawada, Y. Okamoto, A. Nakajiama, and S. Igari, Appl. Phys. A **69**, 179 (1999).
[10]E. Yablonovitch and G. Cody, IEEE Trans. Electron Devices **29**, 300 (1982).
[11]H. W. Deckman, C. B. Roxlo, and E. Yablonovitch, Opt. Lett. **8**, 491 (1983).
[12]O. Kluth, B. Rech, L. Houben, S. Wieder, G. Schöpe, C. Beneking, H. Wagner, A. Löffl, and H. W. Schock, Thin Solid Films **351**, 247 (1999).
[13]C. Rocktuhl, S. Fahr, F. Lederer, K. Bittkau, T. Beckers, and R. Carius, Appl. Phys. Lett. **93**, 061105 (2008).
[14]K. Bittkau, T. Beckers, S. Fahr, C. Rockstuhl, F. Lederer, and R. Carius, Phys. Status Solidi A **205**, 2766 (2008).
[15]R. H. Franken, R. L. Stolk, H. Li, C. H. M. Van der Werf, J. K. Rath, and R. E. I. Schropp, J. Appl. Phys. **102**, 014503 (2007).
[16]H. Li, R. H. Franken, R. L. Stolk, J. A. Schuttauf, C. H. M. Van der Werf, J. K. Rath, and R. E. I. Schropp, J. Non-Cryst. Solids **354**, 2445 (2008).
[17]S. Koynov, M. S. Brandt, and M. Stutzmann, Appl. Phys. Lett. **88**, 203107 (2006).
[18]S. Koynov, M. S. Brandt, and M. Stutzmann, Phys. Status Solidi (RRL) **1**, R53 (2007).
[19]O. Vetterl, F. Finger, R. Carius, P. Hapke, L. Houben, O. Kluth, A. Lambertz, A. Muck, B. Rech, and H. Wagner, Sol. Energy Mater. Sol. Cells **62**, 97 (2000).
[20]S. Guha and J. Yang, J. Non-Cryst. Solids **352**, 1917 (2006).
[21]I. Horcas, R. Fernandez, J. M. Gomez-Rodriguez, J. Colchero, J. Gomez-Herrero, and A. M. Baro, Rev. Sci. Instrum. **78**, 013705 (2007).
[22]R. Swanepoel, J. Phys. E **16**, 1214 (1983).
[23]D. R. G. Rodley, D. I. Jones, and A. D. Stewart, Philos. Mag. Lett. **59**, 149 (1989).
[24]M. S. Brandt, A. Asano, and M. Stutzmann, Mater. Res. Soc. Symp. Proc. **297**, 201 (1993).
[25]R. B. Stephens and G. D. Cody, Thin Solid Films **45**, 19 (1977).
[26]X. Li and P. W. Bohn, Appl. Phys. Lett. **77**, 2572 (2000).
[27]M. Stutzmann, M. C. Rossi, and M. S. Brandt, Phys. Rev. B **50**, 11592 (1994).